technical transactions

No. 2021/004

environmental engineering

sciendo

Mixing effects in the river downstream from pollution discharge point

Andrzej Bielski

abielski@riad.usk.pk.edu.pl | https://orcid.org/0000-0001-5703-0348

Department of Water Supply, Sewerage and Environmental Monitoring, Faculty of Environmental Engineering, Cracow University of Technology

Scientific Editor: Michał Zielina, Cracow University of Technology
Technical Editor: Aleksandra Urzędowska, Cracow University of Technology Press
Language Editor: Tim Churcher, Big Picture
Typesetting: Anna Basista, Cracow University of Technology Press

Received: December 11, 2018
Accepted: March 1, 2021

Copyright: © 2021 Bielski. This is an open access article distributed under the terms of the Creative Commons Attribution License, which permits unrestricted use, distribution, and reproduction in any medium, provided the original author and source are credited.

Data Availability Statement: All relevant data are within the paper and its Supporting Information files.

Competing interests: The authors have declared that no competing interests exist.

Citation: Bielski, A. (2021). Mixing effects in the river downstream from pollution discharge point. *Technical Transactions, e2021004*. https://doi.org/10.37705/TechTrans/e2021004

Abstract

This paper follows the propagation of pollution in a river with a rectangular cross-section of the river bed and a variable cross-sectional velocity. The calculations were made for steady flows and steady pollutant concentrations. To approximate the velocity distribution in the river bed a set of equations for current and vorticity functions was solved. The distribution of pollutant concentrations in the river was calculated from a bidirectional advection and turbulent diffusion equation. Analysis of the distribution of concentrations leads to the conclusion that the effects of transverse advection associated with a lateral inflow of pollutants disappear relatively quickly. Therefore, the distribution of concentrations in cross sections further downstream from the point of pollutant discharge can be determined quite accurately just from an advection-diffusion model, with no transverse advection effects included. Such a level of accuracy is usually sufficient to assess the impact of a pollution source on the aquatic environment. The transverse mixing of pollutants in the stream proceeds slowly and creates a large mixing zone in which the concentrations of pollutants (low but still significant for water quality) can be detected in cross-sections that are remote from the pollutant discharge point. Transverse advection may be ignored while calculating concentrations in remote cross sections at straight watercourse sections and in steady state conditions.

Keywords: pollution, mixing, river, point sources, velocity distribution, concentration distribution

1. Introduction

Pollutants in surface waters undergo many physical, chemical and biochemical processes which affect their ultimate concentrations. Mixing occurs in close proximity to the pollutant discharge point as a result of three-dimensional turbulent diffusion (molecular diffusion is not important in this case) running simultaneously with three-dimensional advection. Further downstream from the discharge point, transverse and vertical advection lose their importance due to viscous inhibition of water volume elements displacement. According to the Directive of the European Parliament (Directive 2008/105/EC), point (19):

In the vicinity of discharges from point sources, concentrations of pollutants are usually higher than the ambient concentrations in water. Therefore, Member States should be able to make use of mixing zones, so long as they do not affect the compliance of the rest of the body of surface water with the relevant EQS. The extent of mixing zones should be restricted to the proximity of the point of discharge and should be proportionate (...). Member States should ensure, as appropriate, that the requirements for the achievement of the environmental objectives set out in Article 4 of that Directive are coordinated for the whole of the river basin district, including the designation of mixing zones in transboundary water bodies...

Article 4 of the Directive (Directive 2008/105/EC) allows violation of water quality standards in mixing zones adjacent to the discharge point, with the provision that:

Concentrations of one or more substances listed in Part A of Annex I may exceed the relevant EQS within such mixing zones if they do not affect the compliance of the rest of the body of surface water with those standards

Mixing close to a source of pollution is a complex issue and it requires that both the velocity field (which changes downstream from the source) and the pollution concentration field are determined. Simplified methods used to study mixing effects have been presented in (Bielski, 2003; 2012a; 2012b; Technical Background, 2010; Jirka, et. al., 2004). These methods assume that there is a constant velocity in the cross section, which may be true at some distance from the river bank. In most cases however pollution sources are located on the river bank where flow velocities drop to practically zero. The changes of velocity within the river's cross section can significantly impact the efficiency of the mixing of pollutants with river water. Additionally, the river bank itself can be seen as a diffusion-impervious barrier that has a significant impact on pollution spreading. In more complicated cases of mixing, calculations can be performed using universal programs, such as CORMIX (CORMIX2, 1991), RMA2 and RMA4 (Surface-water Modeling System), (Donnell, et. al., 2011), Visual Plumes (Frick, et. al., 2003), (Surface Water Models) and HEC – RAS (HEC – RAS, 2016). All of these use numerous data and are thus time-consuming. In some specific cases, simpler calculation methods can be used e.g. when both the river and the entering stream have a steady flow or for a lateral discharge of pollutants and a predominant longitudinal river velocity. The final results may be sufficient to evaluate the impact of the pollution source on the aquatic environment. The article proposes a simplified method of calculating the effects of mixing pollutants with water and determining the concentration field.

In the European Union countries, different formulas are used to estimate the required length L of a mixing zone (Technical Background, 2010; Technical guidelines, 2010; Ceka, 2011):

- the Netherlands, Austria and Sweden: L = 10 * S, no more than 1000 m, (S – width of a river [m])
- Slovakia: for rivers with S up to 100 m, L = 10 * S, no more than 1000 m; for rivers with S above 100 m, L = 10 * S

https://doi.org/10.37705/TechTrans/e2021004

- Sweden: for small rivers, canals and ditches: L = 10 * S, no more than 1000 m, to meet the AA-EQS standards (Directive 2013/39/EU) and L = 0.25 * S no more than 25 m, to meet the MAC-EQS standards (Directive 2013/39/EU)
- Germany: $L = a * S$; a – coefficient ranging from 1 to 5.

In addition, in some countries a criterion for a mixing zone size has been introduced and its width is specified to ensure the free migration of fish:

- the Netherlands: the maximum width is 25% of the wet cross section
- Sweden: the width is 100 m for large water bodies (lakes)
- Germany: the width is calculated as $a * B$, (B – width of river [m], a – coefficient taking the values from 0.1 to 0.5)

In the Netherlands (Ceka, 2011) it is assumed that the length of a mixing zone in large bodies of water (lakes, seas) should be $0.25 * [A/(L/B)]^{0.5}$ (A – area of lake, L – length of lake, B – width of lake); however, $L \leq 1000$ m and $B \leq 100$ m.

The magnitudes of mixing zones proposed in this work will be compared with model calculations. The applied methods of numerical calculations and the analysis of the obtained results are an original extension of the current state of knowledge.

2. Material and Methods

2.1. Velocity field near source of pollution

Approximate water velocities in a horizontal flat motion can be determined with a set of equations combining (HEC – RAS, 2016; Wesseling, 2000; Donnell, et. al., 2001; Holtschlag, Koschik, 2002; Pinho, et. al., 2015):

- continuity equations for an incompressible liquid (if the river depth h changes only slightly):

$$\frac{\partial V_x}{\partial x} + \frac{\partial V_y}{\partial y} = 0 \tag{1}$$

- momentum conservation equations:

$$\frac{\partial V_x}{\partial t} + V_x \frac{\partial V_x}{\partial x} + V_y \frac{\partial V_x}{\partial y} = f_x - \frac{1}{\rho}\frac{\partial p}{\partial x} + (\nu + \nu_T)\cdot\left(\frac{\partial^2 V_x}{\partial x^2} + \frac{\partial^2 V_x}{\partial y^2}\right) - c_f V_x \tag{2}$$

$$\frac{\partial V_y}{\partial t} + V_x \frac{\partial V_y}{\partial x} + V_y \frac{\partial V_y}{\partial y} = f_y - \frac{1}{\rho}\frac{\partial p}{\partial y} + (\nu + \nu_T)\cdot\left(\frac{\partial^2 V_y}{\partial x^2} + \frac{\partial^2 V_y}{\partial y^2}\right) - c_f V_y \tag{3}$$

where:

V_x – horizontal speed component in the direction of the axis 0X→ following the river axis [m/s]
V_y – horizontal speed component in the direction of the axis 0Y→ perpendicular to the axis 0X→ [m/s]
x – coordinate in the direction of the axis 0X→ [m]
y – coordinate in the direction of the axis 0Y→ [m]
ρ – liquid density [g/m^3]
p – hydrostatic pressure, $p = p_0 + h \cdot \rho \cdot g$, [g/(m·s^2)]
h – river depth [m]
p_0 – surface pressure [g/(m·s^2)]
g – acceleration of gravity g = 9.81 m/s^2
f_x, f_y – unit mass forces in a direction of the axis 0X→, 0Y, $f_x = -g \cdot \partial z/\partial x, f_y = -g\cdot\cdot\ \partial z/\partial y$, [m/s^2]
z – bottom elevation [m]

p – hydrostatic pressure, $p = p_0 + h \cdot \rho \cdot g$
ν – kinematic coefficient of viscosity [m²/s]
ν_T – kinematic coefficient of turbulent viscosity [m²/s]
c_f – coefficient of bottom friction, $c_f = n^2 g V / R_h^{4/3}$, $V = (V_x^2 + V_y^2)^{0.5}$, [s^{-1}]
n – roughness coefficient in the Manning formula [m$^{-1/3}$·s]
R_h – hydraulic radius [m]
t – time [s]

For the river, the set of equations (2) and (3) can be written as follows:

$$\frac{\partial V_x}{\partial t} + V_x \frac{\partial V_x}{\partial x} + V_y \frac{\partial V_x}{\partial y} = -g \frac{\partial H}{\partial x} + (\nu + \nu_T) \cdot \left(\frac{\partial^2 V_x}{\partial x^2} + \frac{\partial^2 V_x}{\partial y^2} \right) - c_f V_x \quad (2a)$$

$$\frac{\partial V_y}{\partial t} + V_x \frac{\partial V_y}{\partial x} + V_y \frac{\partial V_y}{\partial y} = -g \frac{\partial H}{\partial y} + (\nu + \nu_T) \cdot \left(\frac{\partial^2 V_y}{\partial x^2} + \frac{\partial^2 V_y}{\partial y^2} \right) - c_f V_y \quad (3a)$$

where:

H – water level elevation, $H = h + z$

While describing a fluid movement, a current function ψ (x, y) is used, which complies with the equation of continuity (1) (Kundu, Cohen, 2002). The relationships between a velocity field and a current function are as follows:

$$V_x = \frac{\partial \psi}{\partial y} \quad (4)$$

$$V_y = -\frac{\partial \psi}{\partial x} \quad (5)$$

ψ – current function [m²/s]

It may be shown that for the vortex field and flat flows (Kundu, Cohen, 2002), the following relationship is true:

$$\frac{\partial V_y}{\partial x} - \frac{\partial V_x}{\partial y} = 2\omega_z = -\xi \quad (6)$$

ω_z – vertical component in the direction of the axis 0Z→ of the angular velocity vector [1/s]
ξ – vortex function [1/s]

A left side of equation (6) is the vertical component of rotation of the velocity field (rot $\vec{V}$).

Using relationships (4) and (5), equation (6) takes the form:

$$\frac{\partial^2 \psi}{\partial x^2} + \frac{\partial^2 \psi}{\partial y^2} = \xi \quad (7)$$

If equation (2) is differentiated with respect to y, while equation (3) with respect to x and then both equations will be subtracted and expressions (4) and (5) will be substituted for V_x and V_y, then the resulting equation depends only on the current function:

$$\frac{\partial}{\partial t}\left(\frac{\partial^2 \psi}{\partial x^2} + \frac{\partial^2 \psi}{\partial y^2} \right) + \frac{\partial \psi}{\partial y} \frac{\partial}{\partial x}\left(\frac{\partial^2 \psi}{\partial x^2} + \frac{\partial^2 \psi}{\partial y^2} \right) - \frac{\partial \psi}{\partial x} \frac{\partial}{\partial y}\left(\frac{\partial^2 \psi}{\partial x^2} + \frac{\partial^2 \psi}{\partial y^2} \right) =$$
$$(\nu + \nu_T) \cdot \left(\frac{\partial^4 \psi}{\partial x^4} + 2\frac{\partial^4 \psi}{\partial x^2 \partial y^2} + \frac{\partial^4 \psi}{\partial y^4} \right) - \frac{\partial (c_f V_x)}{\partial y} + \frac{\partial (c_f V_y)}{\partial x} \quad (8)$$

https://doi.org/10.37705/TechTrans/e2021004

Because equation (8), as a fourth degree equation, is hard to solve with numeric integration methods, it may be written as the following set of equations:

$$\frac{\partial^2 \psi}{\partial x^2} + \frac{\partial^2 \psi}{\partial y^2} = \xi \tag{9}$$

$$\frac{\partial \xi}{\partial t} + \frac{\partial \psi}{\partial y}\frac{\partial \xi}{\partial x} - \frac{\partial \psi}{\partial x}\frac{\partial \xi}{\partial y} = (\nu + \nu_T)\cdot\left(\frac{\partial^2 \xi}{\partial x^2} + \frac{\partial^2 \xi}{\partial y^2}\right) - \frac{\partial (c_f V_x)}{\partial y} + \frac{\partial (c_f V_y)}{\partial x} \tag{10}$$

(eq. (9) is the same as eq. (7)).

In steady states, the derivative with respect to time is reset to zero in equation (10). In steady states, the lack of nonlinear components related to advection and friction resistance in equation (10) results in the following biharmonic equation:

$$\frac{\partial^2 \xi}{\partial x^2} + \frac{\partial^2 \xi}{\partial y^2} = 0 \tag{11}$$

Equations (9) and (11) will be used to determine the approximate velocity field near the pollution source. The field will be assumed as the initial field when solving the set of equations (9) and (10).

2.2. Mass transport model

The differential equation describing the advection transport of pollutants along the watercourse, including longitudinal and transverse turbulent diffusion in transient states, is as follows (Ramaswami, et. al., 2005; Vedat Batu, 2006; Martin, McCutcheon, 1999):

$$\frac{\partial c}{\partial t} + \frac{\partial (V_x \cdot c)}{\partial x} + \frac{\partial (V_y \cdot c)}{\partial y} = \frac{\partial}{\partial x}\left((D + D_{xx})\cdot\frac{\partial c}{\partial x} + D_{xy}\cdot\frac{\partial c}{\partial y}\right) + \frac{\partial}{\partial y}\left((D + D_{yy})\cdot\frac{\partial c}{\partial y} + D_{yx}\cdot\frac{\partial c}{\partial x}\right) \tag{12}$$

where:

c – pollutant concentration [g/m^3]
D – molecular diffusion coefficient [m^2/s]
D_{xx}, D_{yy}, D_{xy}, D_{yx} – turbulent diffusion coefficient [m^2/s]

(other abbreviations as defined above)

Because the components of the velocity field comply with the equation of continuity (1), equation (12) can be simplified to:

$$\frac{\partial c}{\partial t} + V_x \frac{\partial c}{\partial x} + V_y \frac{\partial c}{\partial y} = \frac{\partial}{\partial x}\left((D + D_{xx})\cdot\frac{\partial c}{\partial x} + D_{xy}\cdot\frac{\partial c}{\partial y}\right) + \frac{\partial}{\partial y}\left((D + D_{yy})\cdot\frac{\partial c}{\partial y} + D_{yx}\cdot\frac{\partial c}{\partial x}\right) \tag{13}$$

A turbulent diffusion stream is usually several orders larger than a molecular diffusion stream; therefore, the coefficient D is ignored in real-life applications of equations (12) and (13). However, a turbulent diffusion may sometimes be as low as a molecular diffusion near to the banks of the body of water. Due to finite dimensions of a numerical grid, the average value of the diffusion coefficient for a given grid (mesh) was determined from turbulent diffusion coefficients.

Turbulent diffusion coefficients D_{xx}, D_{yy}, D_{xy} and D_{yx} are related to diffusion coefficients in the main directions D_{TL} (diffusion in the direction of the velocity vector $\vec{V}$) and D_{TH} (diffusion in a direction perpendicular to the velocity vector $\vec{V}$).

2.3. Diffusion and kinematic turbulent viscosity

Turbulent diffusion coefficients can be calculated from formulas with linear dimensions that are characteristic for a riverbed (e.g. average depth h) and dynamic velocity V^* associated with shear stresses observed at a river bottom. The average vertical diffusion coefficient D_{TL} in the direction of the velocity vector $\vec{V}$, can be calculated from formula (Rutherford, 1994):

$$D_{TL} = 0.067 \cdot h \cdot V^* \tag{14}$$

h – river depth [m]
V^* – dynamic velocity [m/s]

The values of turbulent diffusion coefficients D_{TH} in a direction perpendicular to the velocity vector $\vec{V}$ are almost twice as big as D_{TL}; usually, it is assumed that (Rutherford, 1994):

$$D_{TH} = 0.13 \cdot h \cdot V^* \tag{15}$$

Formulas (14) and (15) were used to estimate local values of turbulent diffusion coefficients D_{xx}, D_{yy}, D_{xy}, D_{yx}.

The dynamic velocity was calculated using the formula:

$$V^* = \sqrt{gR_h I} \tag{16}$$

R_h – hydraulic radius [m]
I – hydraulic head loss
g – acceleration of gravity [9.81 m/s^2]

Hydraulic head loss was calculated using the Manning formula:

$$I = \left(V \Big/ \left(\frac{1}{n} R_h^{2/3} \right) \right)^2 \tag{17}$$

n – roughness coefficient [m$^{-1/3}$·s]
($R_h \approx h$ for wide rivers)

From equations (16) and (17):

$$V^* = \sqrt{g R_h^{-1/3}} \cdot n \cdot V \tag{18}$$

V – value of the velocity vector module $\left|\vec{V}\right|$, $V = \sqrt{V_x^2 + V_y^2}$, [m/s]

If formula (18) is introduced to equations (14) and (15) then:

$$D_{TL} = 0.067 \cdot h \cdot \sqrt{g R_h^{-1/3}} \cdot n \cdot V \equiv \alpha_L \cdot V \tag{19}$$

$$D_{TH} = 0.13 \cdot h \cdot \sqrt{g R_h^{-1/3}} \cdot n \cdot V \equiv \alpha_H \cdot V \tag{20}$$

α_L, α_H – diffusivity coefficients [m]

Turbulent diffusion coefficients can be calculated from the following formulas (Ramaswami, et. al., 2005; Vedat Batu, 2006; Myung Eun Lee, Il Won Seo, 2010):

$$D_{xx} = \alpha_L \cdot \frac{V_x^2}{V} + \alpha_H \cdot \frac{V_y^2}{V} \tag{21}$$

$$D_{yy} = \alpha_L \cdot \frac{V_y^2}{V} + \alpha_H \cdot \frac{V_x^2}{V} \tag{22}$$

$$D_{xy} = D_{yx} = (\alpha_L - \alpha_H) \cdot \frac{V_x V_y}{V} \tag{23}$$

https://doi.org/10.37705/TechTrans/e2021004

A kinematic turbulent viscosity can be calculated from formula (HEC – RAS, 2016; Wesseling, 2000):

$$\nu_T = \alpha_T \cdot h \cdot V^* \tag{24}$$

α_T – proportionality ratio (HEC – RAS, 2016):
α_T = 0.11 to 0.26, straight channel, smooth surface
α_T = 0.30 to 0.77, gently meandering channel, moderate surface irregularities
α_T = 2.0 to 5.0, strong meanders, rough surface
(other abbreviations as defined above)

3. Integration of mass flow and mass transport model

The flow model represented by equations (9), (10), (11) was numerically integrated. Differential schemes proposed by the author for these three equations are presented in Appendix I. Central differential quotients were used to approximate the derivatives of the current function ψ and the function of vorticity ξ. Differential equations were solved by the under-relaxation method. The solution of the model made it possible to determine the velocity field necessary for mass propagation calculations.

The mass transport model (13) was also numerically integrated. The differential schemes for this model proposed by the author are described in Appendix II. Backward differential quotients were used to approximate the advection components and central differential quotients to approximate the diffusion components. The integration procedure was carried out in two stages: first, integration in the $0X^{\rightarrow}$ axis direction, then in the $0Y^{\rightarrow}$ axis direction. The sign of the differential quotients of the advection component were changed depending on the sign of the component of the velocity vector.

4. Area of the study

Simulation calculations for the current function ψ and the vorticity function ξ were performed for a strait segment of the river bed with a rectangular cross section and a lateral inflow intersecting the river axis at a 90° angle (Fig. 1).

The values of the current function calculated in the nodes of the numerical grid enabled calculation of the velocity components V_x and ς_ψ from formulas (4) and (5).

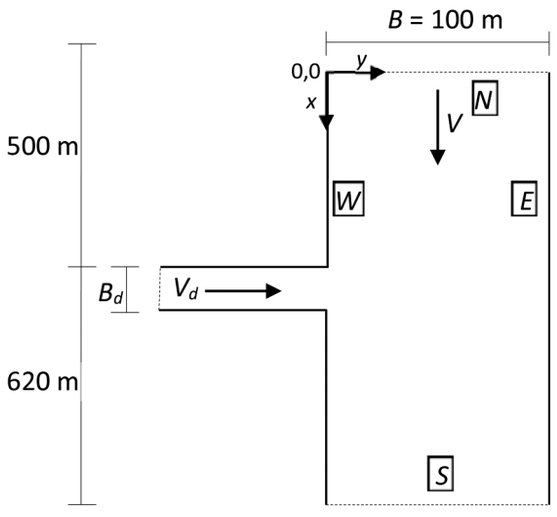

Fig. 1. Layout of the river and its lateral inflow (V – river velocity, V_d – lateral inflow velocity, B – width of the river bed, B_d – width of the lateral inflow, N, W, S, E – the four cardinal directions)

The calculations assume that $R_h \approx h$ = 1 m and n = 0.03 $m^{-1/3}$·s. Therefore, from equation (18):

$$V^* = 0.09396 \cdot V \tag{25}$$

After entering formula (25) into equations (14) and (15) and assuming the values of the parameters:

$$D_{TL} = 0.006295 \cdot V \equiv \alpha_L \cdot V \tag{26}$$

$$D_{TH} = 0.01221 \cdot V \equiv \alpha_H \cdot V \tag{27}$$

The velocity in the initial cross section of the river (x = 0) had a parabolic shape:

$$V(y) = -0.0004 \cdot y \cdot (y - 100)\ \mathrm{m/s},\ y = [\mathrm{m}] \tag{28}$$

A velocity at the inflow point (y = 0) had discrete distributions (29), (30) and (31) for B_d = 24 m, B_d = 8 m and B_d = 6 m, respectively.

$$V_d(x) = \begin{Bmatrix} 0.0\ \mathrm{m/s}, & x = 498\ \mathrm{m} \\ 0.0675\ \mathrm{m/s}, & x = 500\ \mathrm{m} \\ 0.255\ \mathrm{m/s}, & x = 502\ \mathrm{m} \\ 0.465\ \mathrm{m/s}, & x = 504\ \mathrm{m} \\ 0.615\ \mathrm{m/s}, & x = 506\ \mathrm{m} \\ 0.705\ \mathrm{m/s}, & x = 508\ \mathrm{m} \\ 0.735\ \mathrm{m/s}, & x = 510\ \mathrm{m} \\ 0.705\ \mathrm{m/s}, & x = 512\ \mathrm{m} \\ 0.615\ \mathrm{m/s}, & x = 514\ \mathrm{m} \\ 0.465\ \mathrm{m/s}, & x = 516\ \mathrm{m} \\ 0.255\ \mathrm{m/s}, & x = 518\ \mathrm{m} \\ 0.0675\ \mathrm{m/s}, & x = 520\ \mathrm{m} \\ 0.0\ \mathrm{m/s}, & x = 522\ \mathrm{m} \end{Bmatrix} \tag{29}$$

$$V_d(x) = \begin{Bmatrix} 0.0\ \mathrm{m/s}, & x = 498\ \mathrm{m} \\ 0.5\ \mathrm{m/s}, & x = 500\ \mathrm{m} \\ 1.0\ \mathrm{m/s}, & x = 502\ \mathrm{m} \\ 0.5\ \mathrm{m/s}, & x = 504\ \mathrm{m} \\ 0.0\ \mathrm{m/s}, & x = 506\ \mathrm{m} \end{Bmatrix} \tag{30}$$

$$V_d(x) = \begin{Bmatrix} 0.0\ \mathrm{m/s}, & x = 498\ \mathrm{m} \\ 0.5\ \mathrm{m/s}, & x = 500\ \mathrm{m} \\ 0.5\ \mathrm{m/s}, & x = 502\ \mathrm{m} \\ 0.0\ \mathrm{m/s}, & x = 504\ \mathrm{m} \end{Bmatrix} \tag{31}$$

The following values were adopted for a kinematic turbulent viscosity: $R_h \approx h$ = 1 m and n = 0.03 $\mathrm{m}^{-1/3}$·s. Therefore, from equation (24) ν_T = 0.028 V.

5. Numeric grid and initial and boundary conditions for the flow and mass transport model

The mass flow and mass transport model was solved for a section of the watercourse which was 1120 m long and 100 m wide. For numerical calculations, the initial and boundary conditions were formulated for the flow model described in Appendix III and for the mass transport model described in Appendix IV. The annexes also specify what conditions must be met by the function of current ψ, the function of vorticity ξ and the function of concentration c on the border of the analysed area.

https://doi.org/10.37705/TechTrans/e2021004

6. Results and Discussion

6.1. Velocity field

Numeric schemes (I.1a), (I.1b), (I.1c) and (I.4) (Appendix I) helped to determine the approximate course of the current line for three different inflows (Figs. 2–4). The inflow parameters are described in the paragraph "Area of study".

Inflow velocities were similar to the river velocity. Depending on the assumed inflow width (B_d), advection effects in the transverse direction (V_y) disappeared approx. 100–300 m (Fig. 2–4) downstream from the inflow, for similar inflow velocities. Further transport of pollutants would be caused mainly by advection and longitudinal diffusion as well as by transverse diffusion. In the case of smaller inflow velocities, the effects of transverse advection would be noticed at even smaller distances downstream from the inflow. Vortices are a characteristic feature of the velocity fields downstream from the inflow. Their sizes decrease along with the inflow at a constant inflow velocity (Figs. 2–4); in the study, the vortices had a longitudinal dimension of around 40 m and a transverse length of around 4 m (Figs. 2 & 3). There was practically no vortexes for the smallest inflow. The vortex size is significantly reduced by bottom friction.

Knowing the current line values, it was possible to determine the velocity components V_x and V_y from formulas (4) and (5). The components are needed to follow the pollutant transport in the river.

For relatively small pollution sources (B_d = 6 m and mean V_d = 0.033 m/s), compared to the river, vortexes downstream from the inflow are practically unobserved and the current lines run almost parallel to the river bank several dozen metres downstream from the inflow (in this study, 20–30 m).

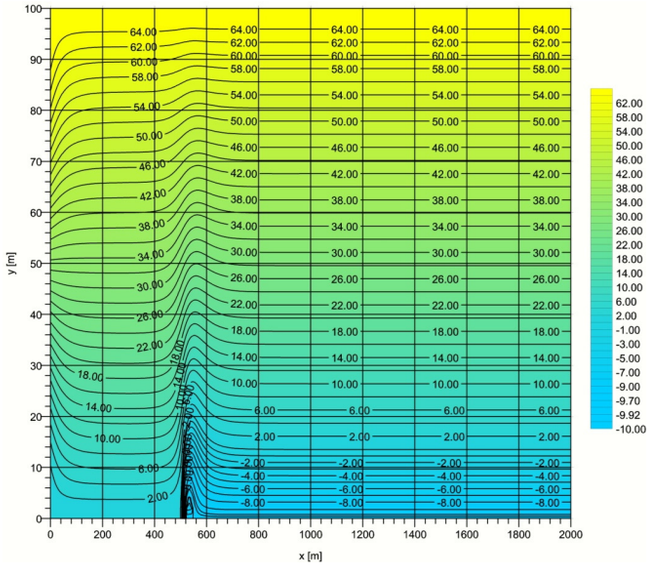

Fig. 2. Current lines for B_d = 24 m (numbers on isolines represent the current line values)

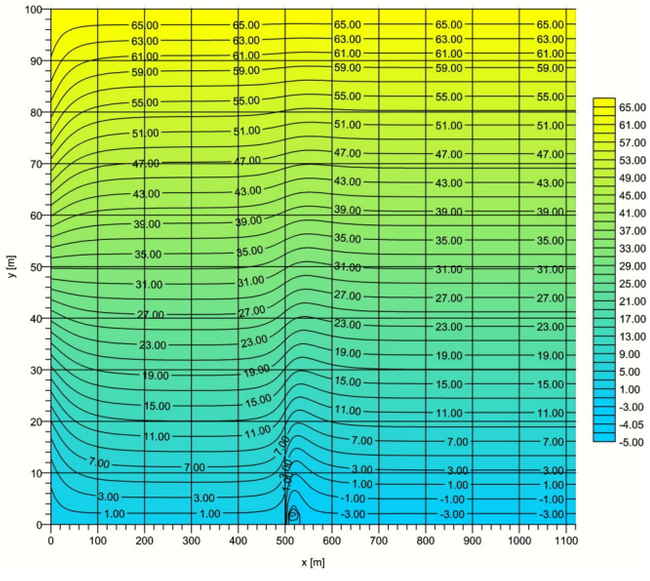

Fig. 3. Current lines for B_d = 8 m (numbers on isolines represent the current line values)

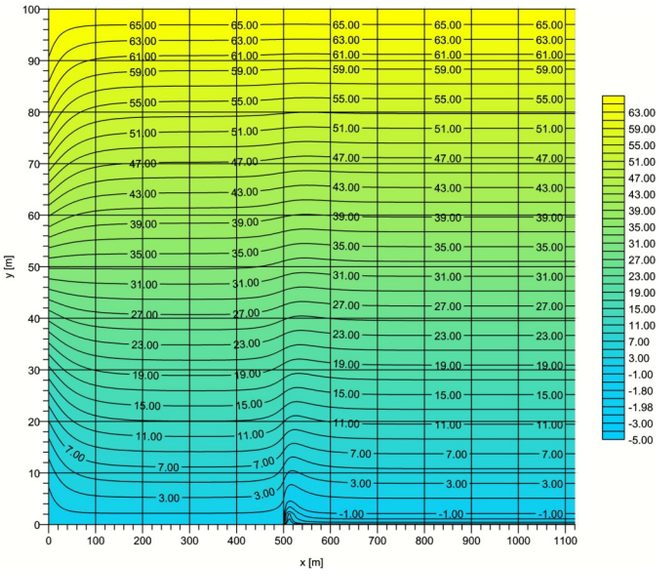

Fig. 4. Current lines for B_d = 6 m (numbers on isolines represent the current line values)

6.2. Concentration field

The numeric scheme (II.1) and (II.2) (Appendix II) helped to determine the distribution of pollutant concentrations in the river for three inflows (Figs. 5–7).

Figures 5–7 represent the concentration propagation in steady state conditions. Molecular and turbulent diffusion is responsible for the dissipation of pollutants in both longitudinal and transverse directions. It should be noted that the highest concentrations of pollutants are observed near the bank where the pollution discharge occurred (Bielski, 2012a). If the pollutants enter the river at a certain distance from the bank, the maximum concentrations always tend to move towards the nearest bank, except for the case when the discharge is located at the river and the velocity field axes (Bielski, 2012a).

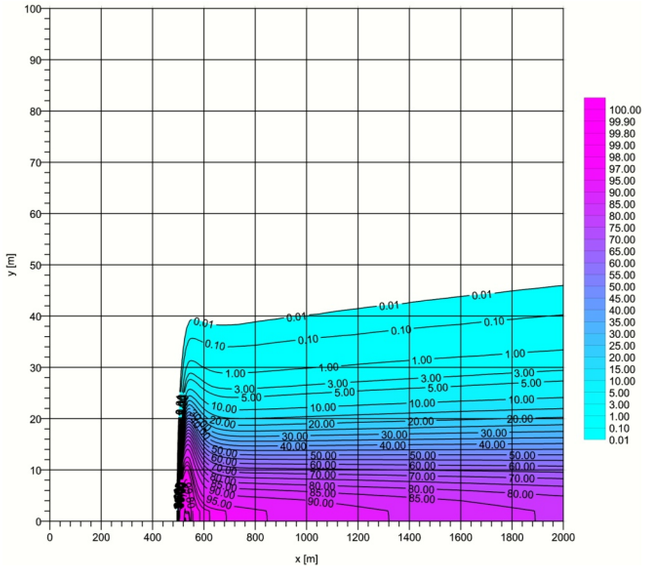

Fig. 5. Distribution of pollutant concentration in the river for B_d = 24 m (numbers on isolines represent concentration)

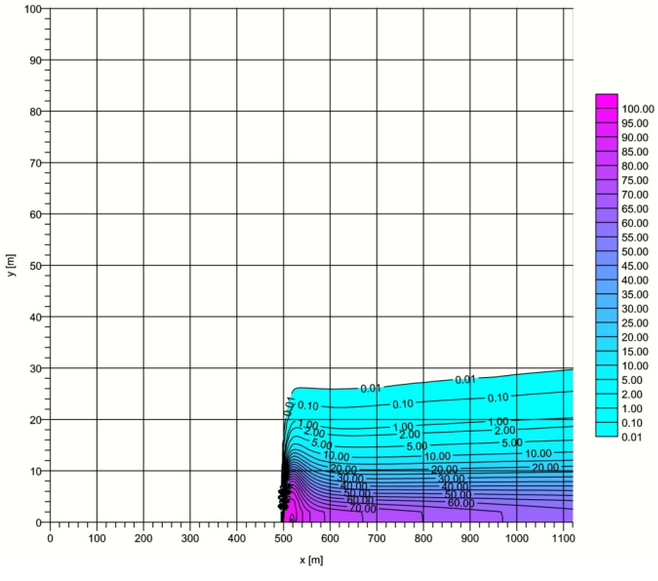

Fig. 6. Distribution of pollutant concentration in the river for B_d = 8 m (numbers on isolines represent concentration)

Concentrations equal to 50% of the inflow concentration (c_d = 100 g/m^3) are located at a distance of approx. δ from the bank. The value results from the mass balance of pollutants entering the river and the pollutants transported by the river and corresponds to a gradual decrease of transverse velocity (in this study, around 100 m downstream from the inflow, Figs. 2–4). This agrees with the rule of diffusion effects which shows that a concentration of 50% of the concentration for a step excitation moves due to advection with no diffusion.

If molecular and turbulent diffusion were not observed, then a concentration distribution in a transverse direction of the river would step change from a maximum of 100 g/m^3 to 0. In the case of an inflow width of B_d = 24 m, the 50% inflow concentration was found around δ = 13 m from the shore (Fig. 5). This distance agrees with the pollutant width calculated for a step profile change of concentration toward a transverse direction of the river, obtained from the mass balance for a diffusion-free flow. For B_d = 8 m and B_d = 6 m, 50% concentrations were located approx. 6 m and 3 m from the bank, respectively (Figs. 6 & 7).

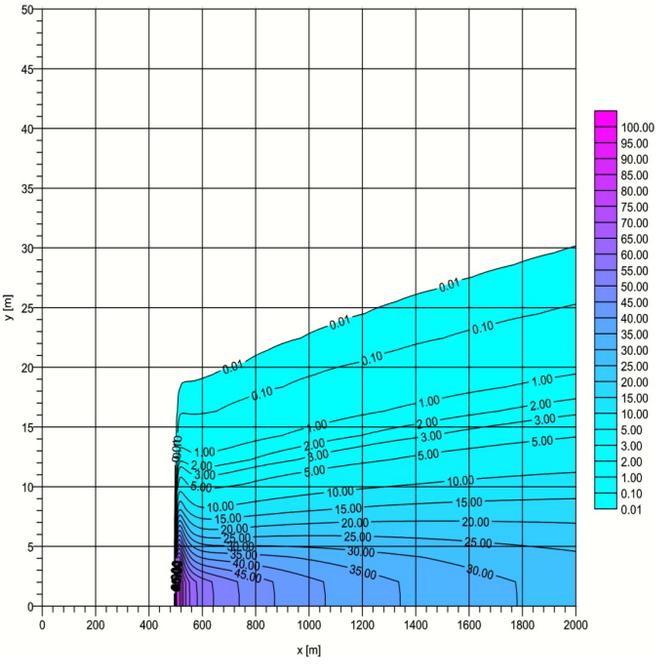

Fig. 7. Distribution of pollutant concentration in the river for B_d = 6 m (numbers on isolines represent concentration)

https://doi.org/10.37705/TechTrans/e2021004

Such distances are consistent with calculations for a rectangular concentration profile obtained from the mass balance for a diffusion-free flow in steady state conditions:

1. Inflow width B_d = 24 m, inflow velocity described by equation (29), numerically determined average river velocity V_x = 0.752 m/s in a cross section x = 1100 m (distance from the pollution source approx. 600 m), river bed coordinates $y \in$ <0, 24> m, distance δ:

$$\delta = \frac{\int_0^{B_d} c_d \cdot V_d(y) \cdot dy \cdot h}{c_d \cdot \bar{V}_x \cdot h} = \frac{S_d \cdot h}{c_d \cdot \bar{V}_x \cdot h} = \frac{S_d}{c_d \cdot \bar{V}_x} = \frac{1000\,\mathrm{g/(m \cdot s)}}{100\,\mathrm{g/m^3} \cdot 0.752\,\mathrm{m/s}} = 13.30\ \mathrm{m} \approx 13\ \mathrm{m}$$

Inflow width B_d = 8 m, inflow velocity described by equation (30), numerically determined average river velocity V_x = 0.663 m/s in a cross section x = 1100 m (distance from the pollution source approx. 600 m), river bed coordinates $y \in$ <0, 14> m , distance δ:

$$\delta = \frac{c_d \cdot V_d \cdot B_d \cdot h}{c_d \cdot \bar{V}_x \cdot h} = \frac{S_d \cdot h}{c_d \cdot \bar{V}_x \cdot h} = \frac{S_d}{c_d \cdot \bar{V}_x} = \frac{400\,\mathrm{g/(m \cdot s)}}{100\,\mathrm{g/m^3} \cdot 0.663\,\mathrm{m/s}} = 6.03\ \mathrm{m} \approx 6\ \mathrm{m}$$

Inflow width B_d = 6 m, inflow velocity described by equation (31), numerically determined average river velocity $\bar{V}_x$ = 0.620 m/s in a cross section x = 1100 m (distance from the pollution source approx. 600 m), river bed coordinates $y \in$ <0, 9> m, distance δ:

$$\delta = \frac{c_d \cdot V_d \cdot B_d \cdot h}{c_d \cdot \bar{V}_x \cdot h} = \frac{S_d \cdot h}{c_d \cdot \bar{V}_x \cdot h} = \frac{S_d}{c_d \cdot \bar{V}_x} = \frac{200\,\mathrm{g/(m \cdot s)}}{100\,\mathrm{g/m^3} \cdot 0.620\,\mathrm{m/s}} = 3.23\ \mathrm{m} \approx 3\ \mathrm{m}$$

The mixing of pollutants with river water occurs at considerable distances from the discharge point. A vortex that is formed downstream from the inflow (Figs. 2–4) intensifies the mixing of pollutants with river water. Figures 8–10 show the concentration distributions for half the width of the river obtained from the two-dimensional model (13) (lines marked as "exact solution" refer to distributions at (x – 500) m from the source, located on the right bank) and approximation lines for cross sections with different values of x (where x is the distance from the source located at the right bank) derived from the advection diffusion model

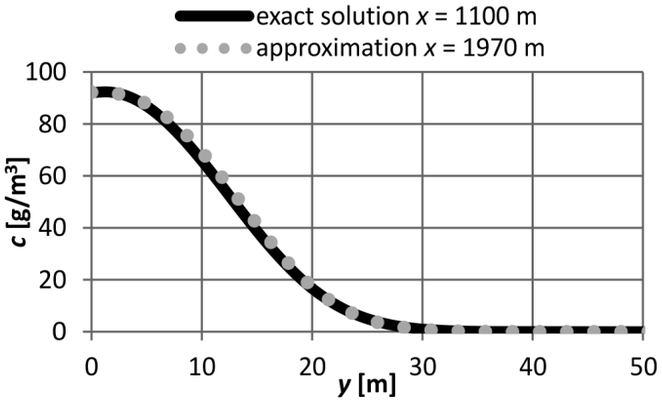

Fig. 8. Concentration distribution resulting from a numeric solution of the advection-diffusion equation vs. approximate distributions for B_d = 24 m, cross section with x = 1100 m (distance from discharge point 600 m) in steady state conditions

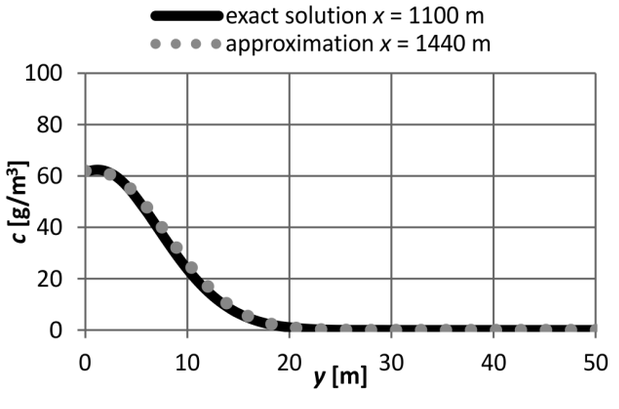

Fig. 9. Concentration distribution resulting from a numeric solution of the advection-diffusion equation vs. approximate distributions for B_d = 8 m, cross section with x = 1100 m (distance from discharge point 600 m) in steady state conditions

type (13) but without a transverse advection (V_y = 0) and coefficients D_{xy} and D_{yx}. The approximate solutions were obtained assuming that at x = 0 m, the river concentration is 100 g/m³ for δ = {13, 6, 3} m. Velocity distributions V_x in these locations were calculated from model (9) and (10) in cross sections x = {1100, 1100, 1100} m for inflow widths B_d = {24, 8, 6} m, respectively. Therefore, pollutant propagations for a rectangular distribution of concentrations of width δ, resulting from the mass balance at the inflow point (without transverse advection and associated turbulent diffusion) give concentration distributions similar to those observed in the two-dimensional model (13) but at different distances from the pollution source: 1970 m (Fig. 8), 1440 m (Fig. 9) and 780 m (Fig. 10). The calculated distance differences are respectively: (1970 – (1100 – 500)) = 1370 m, (1440 – (1100 – 500)) = 840 m, (780 – (1100 – 500)) = 180 m.

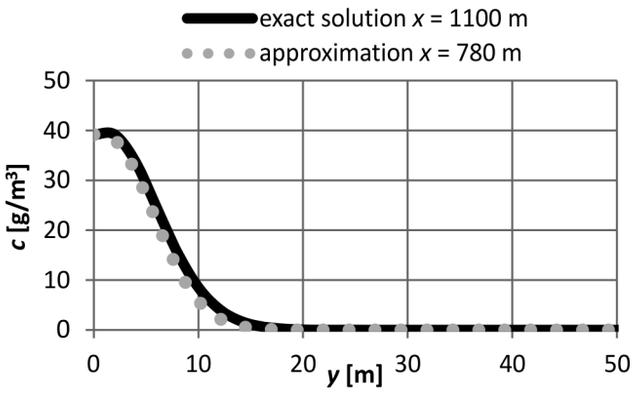

Fig. 10. Concentration distribution resulting from a numeric solution of the advection-diffusion equation vs. approximate distributions for B_d = 6 m, cross section with x = 1100 m (distance from discharge point 600 m) in steady state conditions

The distance where similar distributions are observed depends on the magnitude of the pollution source, described by such features as inflow width, inflow velocity, geometry of the channel or bed of the entering lateral inflow in relation to the characteristics of the river. The smaller the source (comparing to the river) the smaller the distances. Therefore, calculations of pollutant propagation with the simplified model (13) for sufficiently small sources, with a rectangular concentration distribution at the pollution source and located within plume of pollutants a width resulting from the mass balance give concentration distributions similar to those obtained from the two-dimensional model (13) at very similar distances from the source. The simplified model (13) makes it easier to find concentration distributions when a lateral inflow of pollution takes place. When analysing concentration distributions further down from the lateral inflow, the magnitude of displacement becomes unimportant.

7. Effects of the transverse mixing of pollutants

The energy of the tributary stream is dissipated relatively quickly in the receiver stream such a river. The range of its impact is so small that concentration distributions in cross sections far from the pollution source vary considerably. This variability is characterised by the coefficient of variation ν, i.e. the ratio of the standard deviation to the average pollutant concentration. The coefficients of variation for the source widths of B_d = 24 m and 6 m (Figs. 5 & 7) in a cross section with x = 2000 m (2000 – 500 = 1500 m from the source) were 1.93 and 2.48, respectively. High coefficient values indicate that a standard deviation contributes significantly to the average value resulting in poor mixing conditions. If the average inflow velocity increased to 3.33 m/s for B_d = 6 m, then the coefficient of variation in a cross section with x = 2000 m would decrease to 1.40. Despite a significant increase in the energy of incoming pollutants, the contribution of the standard deviation to the average concentration is still high, reaching 140%. Therefore, an effective mixing of pollutants with the river water is not possible by merely increasing the inflow velocity.

According to the Dutch guidelines (Ceka, 2011), the concentrations of, for example, zinc or copper should not exceed the maximum allowable concentration by more than 0.1 or the local background concentration by more than 10% at the end of the mixing zone.

In the analysed case, the length of the mixing zone is 1000 m (10*100 m), according to the guidelines (Technical Background, 2010; Technical guidelines, 2010; Ceka, 2011).

If the background concentrations were only half of the inflow concentration, i.e. 50 g/m³, then the concentration at the zone border should not exceed 55 g/m³; for B_d = 6 m, the maximum concentration at the zone border was

https://doi.org/10.37705/TechTrans/e2021004

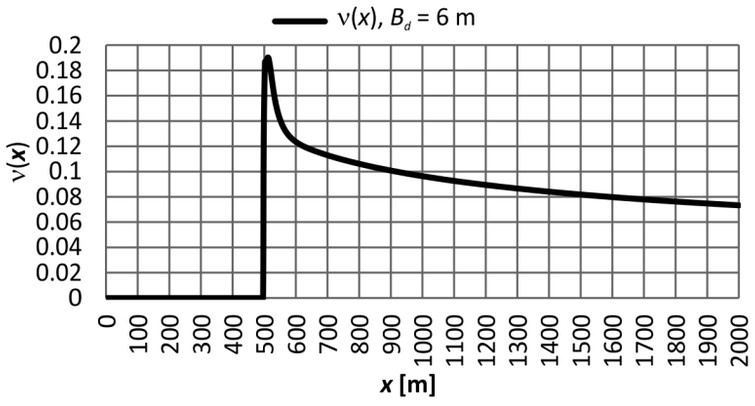

Fig. 11. Distribution of the coefficient of variation ν(*x*) of pollutant concentrations for B_d = 6 m (pollution load per unit depth 200 g/(m·s); background concentration 50 g/m³)

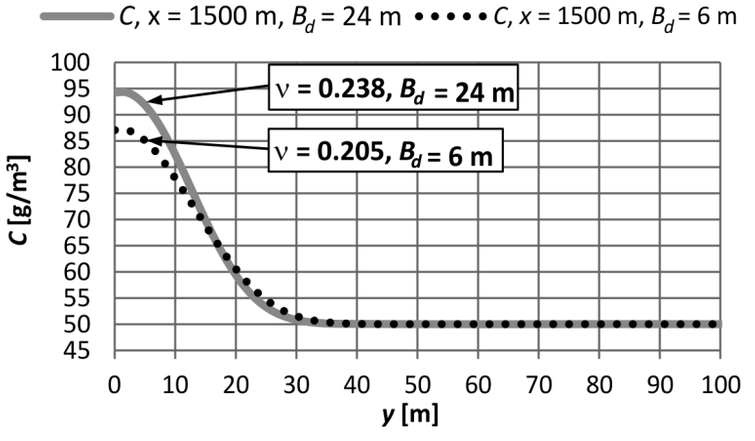

Fig. 12. Distribution of pollutant concentrations in a cross section with *x* = 1500 m (1000 m from the pollution source); B_d = {24,6} m

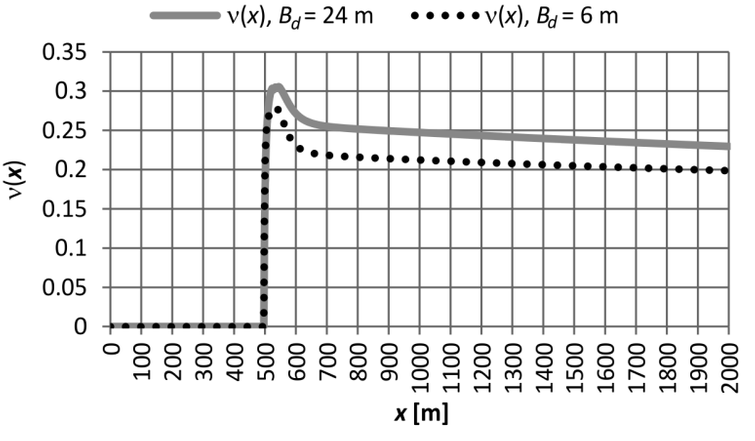

Fig. 13. Distribution of the coefficient of variation ν(*x*) of pollutant concentration for B_d = {24,6} m (pollution load per unit of depth 1000 g/(m·s); background concentration 50 g/m³)

66.72 g/m³, so it exceeded the background concentrations by over 10%. It should be noted, however, that the coefficient of variation was only 0.082 (cross section with x = 1500 m), which indicates that concentrations start to level in this cross section (Fig. 11). Thus, exceedance of the background concentration as well as the equalisation of the concentration distribution will be determined not only by the energy of incoming pollutants but also by the background concentration. However, it should be noted that if the inflow concentration and the background concentration are similar, then low unevenness coefficients of a concentration distribution in a given cross section do not necessarily prove the occurrence of good mixing conditions.

Introduction of the same pollution load, i.e. 1000 g/(m·s) (a background concentration of 50 g/m³), but from a source four times smaller and with a velocity four times higher (1.67 m/s) does not essentially improve mixing effects (Fig. 12). The coefficient of variation 1000 m downstream from source with B_d = 24 m is reduced from ν = 0.238 to ν = 0.205 for source with B_d = 6 m (Fig. 12). A higher transverse velocity near laterals slightly improved the mixing effects along 1500 m of the bank (Fig. 13). The changes of the coefficient of variation ν observed along the watercourse for two pollution sources (Fig. 13) indicated that changes of were more significant near the sources (*x* = 500 m) than in remote cross sections. Such big changes of ν close to the sources (Fig. 13) are caused by the high energy of incoming streams. Their energy is quickly dissipated as a result of friction and thermal effects, resulting in a slow decrease of the coefficient ν downstream from the sources (Fig. 13). In order for energy to provide satisfactory mixing effects, the inflow velocities would have to be much higher, which would be economically unprofitable and hard to implement in practice.

The increase of the inflow velocity results in faster movements of water volume elements, higher turbulent diffusion coefficients and higher momentum dispersion. This only improves mixing effects close to the inflow source. In cross sections located over 150–200 m from the source, the mixing effects are mainly related to turbulent dispersion generated by the longitudinal velocity component. These mixing effects are not very intensive and therefore the coefficient of variation ν(*x*) decreases slowly downstream from the source (Fig. 13).

8. Conclusions

1. The approximate velocity field can be derived from the set of equations (9) and (10) using an explicit numeric scheme for the vorticity function and an implicit numeric scheme for the current function.

2. A relatively quick approximate method of convergence can be used to determine the current function by an implicit numeric scheme; the calculations required around 50 iterations.
3. In steady states in surface waters with lateral inflows (for flow velocities V = 1 m/s) a disappearance of a transverse advection is observed in sections located about 100 to 300 m downstream from the inflow. This distance is shorter for lower inflow velocities and when viscous and frictional effects inhibiting advection and vorticity motion are taken into account.
4. In steady states, the highest concentrations of pollutants in a given cross section are always observed near the bank where the lateral inflow is located, with the maximum concentration always found at the bank. When a pollutant discharge takes place at a certain distance from the bank (except for the river axis and the velocity field axis) the maximum concentrations always tend to move towards the closest bank.
5. It is possible to establish an approximate distribution of concentrations in the watercourse with the lateral inflow of pollutants using the advection-diffusion equation, in which transverse advection and components describing the effects of turbulent diffusion related to transverse advection are ignored. For rather small sources, a concentration distribution will concern the cross section shifted by the distance equal to the length of the section along which the transverse advection disappears.
6. In steady states, the approximated width of the pollution zone where concentrations exceed 50% of the inflow concentration can be estimated from the mass balance of pollutants in the inflow and in the watercourse. The width involves the cross section located far from the pollution source where there is no transverse advection caused by the side inflow.
7. The effective mixing of pollutants with the receiving water cannot be achieved by merely increasing the inflow velocity.
8. When assessing the mixing effects using simulations, the background pollution concentration should be assumed to be zero. The adoption of non-zero background concentrations contributes to the equalisation of a transversal distribution of concentrations, which leads to a false conclusion (good mixing conditions).
9. It is difficult to obtain accurate concentration distribution calculations due to the following factors: irregularities in natural channel surfaces, flow changes in both the watercourse and the lateral inflow, different river bed characteristic, variability of pollutant loads, variability of physical and chemical processes rates, changes of water temperatures, etc.. The approximate steady states calculations presented in this paper may in many cases be quite sufficient from the perspective of surface water protection. The impact of the pollution source on the aquatic environment is usually studied for low water levels while in actuality, the surface water levels are constantly changing. Therefore, even exact calculations only approximate the actual distribution of pollution concentrations in the watercourse.
10. The set of equations of a flat velocity field model can be solved using an explicit differential scheme for the vortex function and an approximation method for a differential scheme of the current function.

Appendix I

Numeric integration of the flow model

In the numeric representation of equations (9) and (11), differential quotients central for the functions ψ and ξ were used. The set of differential equations was solved using an under- relaxation method until the maximum relative error of the solution for ψ and ξ was lower than ε = 10-10. In the following approximations, the new values ψ new and ξ new were calculated from the formulas:

https://doi.org/10.37705/TechTrans/e2021004

$$\left(\frac{\psi_{i+1,j}^{\text{old}}+\psi_{i-1,j}^{\text{old}}}{\Delta x^2}+\frac{\psi_{i,j+1}^{\text{old}}+\psi_{i,j-1}^{\text{old}}}{\Delta y^2}-\xi_{i,j}^{\text{old}}\right)\frac{1}{2/\Delta x^2+2/\Delta y^2}=\psi_{i,j} \tag{I.1a}$$

$$\psi_{i,j}^{\text{new}}=\psi_{i,j}^{\text{old}}+\alpha_{\psi}\left(\psi_{i,j}-\psi_{i,j}^{\text{old}}\right) \tag{I.1b}$$

$$\psi_{i,j}^{\text{old}}=\psi_{i,j}^{\text{new}} \tag{I.1c}$$

$$\left(\frac{\xi_{i+1,j}^{\text{old}}+\xi_{i-1,j}^{\text{old}}}{\Delta x^2}+\frac{\xi_{i,j+1}^{\text{old}}+\xi_{i,j-1}^{\text{old}}}{\Delta y^2}\right)\frac{1}{2/\Delta x^2+2/\Delta y^2}=\xi_{i,j} \tag{I.2a}$$

$$\xi_{i,j}^{\text{new}}=\xi_{i,j}^{\text{old}}+\alpha_{\xi}\left(\xi_{i,j}-\xi_{i,j}^{\text{old}}\right) \tag{I.2b}$$

$$\xi_{i,j}^{\text{old}}=\xi_{i,j}^{\text{new}} \tag{I.2c}$$

where:

$\psi_{\ldots\ldots}^{\text{old}}$, $\xi_{\ldots\ldots}^{\text{old}}$ – values of current and vorticity functions from the previous approximation

$\psi_{\ldots\ldots}^{\text{new}}$, $\xi_{\ldots\ldots}^{\text{new}}$ – values of current and vorticity functions for the new approximation

α_{ψ} – under relaxation coefficient for ψ, assumed $\alpha_{\psi}=0.9$

α_{ξ} – under relaxation coefficient for ξ, assumed $\alpha_{\xi}=0.01$

i – index related to the direction of the axis $0X^{\rightarrow}$

j – index related to the direction of the axis $0Y^{\rightarrow}$

Δx, Δy – dimensions of a numeric grid in the direction of the axis $0X^{\rightarrow}$ and 0Y, respectively

Calculations for the values of the functions ψ and ξ were completed when:

$$\left(\psi_{i,j}^{\text{new}}-\psi_{i,j}\right)/\psi_{i,j}\le\varepsilon \tag{I.3a}$$

$$\left(\xi_{i,j}^{\text{new}}-\xi_{i,j}\right)/\xi_{i,j}\le\varepsilon \tag{I.3b}$$

In the numeric integration of equations (9) and (10), numeric schemes (25a), (25b) and (25c) were used for the current function Ψ while for the vorticity function ξ the scheme resulting from equation (10) was employed:

$$\begin{aligned}\xi_{i,j}^{k+1}=\xi_{i,j}^{k+1}&+(\nu+\nu_{T,i,j})\cdot\left(\frac{\xi_{i+1,j}^{k}-2\xi_{i,j}^{k}+\xi_{i-1,j}^{k}}{\Delta x^2}+\frac{\xi_{i,j+1}^{k}-2\xi_{i,j}^{k}+\xi_{i,j-1}^{k}}{\Delta y^2}\right)\cdot\Delta t\\&-(V_{x,i,j}\ge 0)\cdot V_{x,i,j}\frac{\xi_{i,j}^{k}-\xi_{i-1,j}^{k}}{\Delta x}\cdot\Delta t\\&-(V_{x,i,j}\le 0)\cdot\left|V_{x,i,j}\right|\frac{\xi_{i,j}^{k}-\xi_{i+1,j}^{k}}{\Delta x}\cdot\Delta t\\&-(V_{y,i,j}\ge 0)\cdot V_{y,i,j}\frac{\xi_{i,j}^{k}-\xi_{i,j-1}^{k}}{\Delta y}\cdot\Delta t\\&-(V_{y,i,j}\le 0)\cdot\left|V_{y,i,j}\right|\frac{\xi_{i,j}^{k}-\xi_{i,j+1}^{k}}{\Delta y}\cdot\Delta t\\&-\frac{c_{f,i,j+1}V_{x,i,j+1}-c_{f,i,j-1}V_{x,i,j-1}}{2\Delta y}\cdot\Delta t\\&+\frac{c_{f,i+1,j}V_{y,i+1,j}-c_{f,i-1,j}V_{y,i-1,j}}{2\Delta x}\cdot\Delta t\end{aligned} \tag{I.4}$$

k – index related to time

$|.....|$ – absolute value

$(.....\geq 0)$, $(.....< 0)$ – numbers assigned to logical evaluations; if the condition is met the value is 1, otherwise it is 0

(other abbreviations are as defined above)

Appendix II

Numeric integration of the mass transport model

Numeric integration of the mass transport model (13) proceeded in two steps, beginning with integration along the axis 0X$^{\rightarrow}$ and then along the axis 0Y$^{\rightarrow}$.

The following formulas were used:

- for the axis 0X$^{\rightarrow}$:

$$\begin{aligned} c_{i,j}^{*,k+1} = c_{i,j}^{k} &- \Delta t \cdot V_{x,i,j} \frac{c_{i,j}^{k} - c_{i-1,j}^{k}}{\Delta x} \cdot \left(V_{x,i,j} \geq 0\right) + \\ &- \Delta t \cdot \left|V_{x,i,j}\right| \frac{c_{i,j}^{k} - c_{i+1,j}^{k}}{\Delta x} \cdot \left(V_{x,i,j} < 0\right) + \\ &+ \Delta t \cdot \frac{D_{xx,i+1,j}\left(c_{i+1,j}^{k} - c_{i,j}^{k}\right) - D_{xx,i,j}\left(c_{i,j}^{k} - c_{i-1,j}^{k}\right)}{\Delta x^{2}} + \\ &+ \Delta t \cdot \frac{D_{xy,i+1,j}\left(c_{i+1,j+1}^{k} - c_{i+1,j-1}^{k}\right) - D_{xy,i-1,j}\left(c_{i-1,j+1}^{k} - c_{i-1,j-1}^{k}\right)}{4 \cdot \Delta x \cdot \Delta y} \end{aligned} \tag{II.1}$$

- for the axis 0Y$^{\rightarrow}$:

$$\begin{aligned} c_{i,j}^{k+1} = c_{i,j}^{*,k+1} &- \Delta t \cdot V_{y,i,j} \frac{c_{i,j}^{*,k+1} - c_{i,j-1}^{*,k+1}}{\Delta y} \cdot \left(V_{y,i,j} \geq 0\right) + \\ &- \Delta t \cdot \left|V_{y,i,j}\right| \frac{c_{i,j}^{*,k+1} - c_{i,j+1}^{*,k+1}}{\Delta y} \cdot \left(V_{y,i,j} < 0\right) + \\ &+ \Delta t \cdot \frac{0.5\left(D_{yy,i,j+1} + D_{yy,i,j}\right)\left(c_{i,j+1}^{*,k+1} - c_{i,j}^{*,k+1}\right) - 0.5\left(D_{yy,i,j} + D_{yy,i,j-1}\right)\left(c_{i,j}^{*,k+1} - c_{i,j-1}^{*,k+1}\right)}{\Delta y^{2}} + \\ &+ \Delta t \cdot \frac{D_{yx,i,j+1}\left(c_{i+1,j+1}^{*,k+1} - c_{i-1,j+1}^{*,k+1}\right) - D_{yx,i,j-1}\left(c_{i+1,j-1}^{*,k+1} - c_{i-1,j-1}^{*,k+1}\right)}{4 \cdot \Delta y \cdot \Delta x} \end{aligned} \tag{II.2}$$

k – index related to time

$|.....|$ – absolute value

$(.....\geq 0)$, $(.....< 0)$ – numbers assigned to logical evaluations; if the condition is met the value is 1, otherwise it is 0

(other abbreviations are as defined above)

https://doi.org/10.37705/TechTrans/e2021004

Appendix III

Numeric grid and initial and boundary conditions for the velocity field

Numeric calculations of a flat flow were conducted for a rectangular area ($0 \le x \le 1120$ m, $0 \le y \le 100$ m). Dimensions of a numeric grid were: $\Delta x = 2$ m and $\Delta y = 2$ m. It was assumed that indexes i of the grid changed from 0 to M along the axis 0X$^{\rightarrow}$, while indexes j changed from 0 to N along the axis 0Y$^{\rightarrow}$. When calculations begin, both $\psi(x, y) = 0$ and $\xi(x, y) = 0$.

The values of the function $\psi(x, y)$ along N, W and E were calculated numerically using a curvilinear integral, directed along the banks where points $l = 1, \ldots, P$ ($l = 0$ – beginning of the curve) were assigned to components of the velocity vector:

$$\psi_l = \psi_{l=0} + \sum_{l=1}^{P} -V_{y,l}\Delta x_l + V_{x,l}\Delta y_l \tag{III.1}$$

For the bank:

- [N]; $V_y = 0$, index l refers to index j of a rectangular grid while $i = 0$
- [W]; $V_x = 0$, $V_y = 0$, except for an inflow section and then $V_y \neq 0$; index l refers to index i, of a rectangular grid while $j = 0$
- [E]; $V_x = 0$, $V_y = 0$, index l refers to index i of a rectangular grid, while $j = \mathrm{N}$

The common points that mark the end of the one section of the bank and the beginning of the another correspond to the same ψ. It was assumed that $\psi\ (x = 0, y = 0) = 0$.

For the bank S, it was athat:

$$\frac{\partial \psi}{\partial x} = 0 \tag{III.2}$$

From the condition (III.2), it may be concluded that current lines run parallel to W and E if perpendicular to S, so $V_y = 0$.

The values of the vorticity function $\xi(x, y)$ for the banks N and S were calculated from the differential quotient:

$$\xi_{i,j} = \frac{\psi_{i,j+1} - 2\psi_{i,j} + \psi_{i,j-1}}{\Delta y^2}, i = \{0, M\}, j = 1, \ldots, N-1 \tag{III.3}$$

(for $j = \{0, N\}$ any values can be used since they are not included in the algorithm; it was assumed that: $\xi_{i,j=0} = 0$, $\xi_{i,j=N} = 0$ and $i = \{0, M\}$).

Formula (III.3) results from equation (7), assuming that when the banks N and S are at a sufficiently large distance from the inflow, the condition (III.2) it true.

The values of a vorticity function $\xi(x, y)$ for the banks W and E were calculated from the differential quotient:

$$\xi_{i,j} = \frac{\psi_{i+1,j} - 2\psi_{i,j} + \psi_{i-1,j}}{\Delta x^2} + \frac{\psi_{i,j+1} - 2\psi_{i,j} + \psi_{i,j-1}}{\Delta y^2}, i = 1, \ldots M, j = \{0, N\} \tag{III.4}$$

under the additional conditions:

$$\psi_{i,j-1} = \psi_{i,j+1}, i = 1, \ldots M, j = 0 \tag{III.5}$$

$$\psi_{i,j+1} = \psi_{i,j-1}, i = 1, \ldots M, j = N \tag{III.6}$$

The conditions (III.5) and (III.6) prove that there is symmetry of the solution along the banks W and E and the derivative is zero:

$$\frac{\partial \psi}{\partial y} = \frac{\Psi_{i,j+1} - \Psi_{i,j-1}}{2\Delta y} = 0 \qquad \text{(III.7)}$$

Moreover, the condition (III.7) indicates that close to the banks W and E ($y = 0^+, y = 0^-$ or $y = B^+, y = B^-$) the function $\psi(x, y)$ has a symmetrical distribution and its minimum value is located at the bank. The value of V_x at the banks W and E results only from a model solution and other boundary conditions; it may or may not be zero although V_x is zero at the banks W and E, according to the condition (III. 7) .

The condition (III.2) also states that a derivative $\partial\xi/\partial x = 0$ in a direction perpendicular to S. It means that vorticity ξdoes not change towards the axis $0X^{\rightarrow}$ around S; ξ is also time dependent (t) in the case of the integration of equation (10).

Appendix IV

Numeric grid and initial and boundary conditions for the concentration field

A pollutant concentration field was calculated for the same area and the same numeric grid as the velocity field. At the beginning of the calculations, it was assumed that $c(x, y) = 0$ outside the banks.

It was also assumed that for the pollutant concentration along the bank N:

$$c(x = 0, y) = 0 \qquad \text{(IV.1)}$$

For the bank S, an approximate condition was accepted as:

$$\frac{\partial c}{\partial x} = \frac{c_{i=M,j} - c_{i=M-1,j}}{\Delta x} = 0 \qquad \text{(IV.2)}$$

The condition (IV.2) shows how diffusion fades away and has a minor impact on the concentration on the bank S.

It was assumed that there was no diffusive permeability through the banks W and E, so a derivative is:

$$\left.\frac{\partial c}{\partial x}\right|_{i,j} = \frac{c_{i,j+1} - c_{i,j}}{\Delta x} = 0 \,, i = 1,...M \,, j = \{-1, N+1\} \qquad \text{(IV.3)}$$

Due to the condition (IV.3):

$$c_{i,j} = c_{i,j+1} \,, i = 1,...M \,, j = -1 \qquad \text{(IV.4)}$$

$$c_{i,j} = c_{i,j-1} \,, i = 1,...M \,, j = N+1 \qquad \text{(IV.5)}$$

The condition (IV.3) and relationships (IV.4) and (IV.5) show that a diffusion stream in a direction normal to the banks W and E reaches zero at these banks (Fick's law).

In addition, it was assumed that along the right bank near the inflow, the concentration:

$$c_d = c(x, y = 0) = 100\,\mathrm{g/m^3}, \; x \in < 500, 500 + B_d > \qquad \text{(IV.6)}$$

https://doi.org/10.37705/TechTrans/e2021004

References

Bielski, A. (2003). Advection with two-way dispersion of pollutants in unsteady state in water environment. *Technical Transactions*, *3*: 347–373.

Bielski, A. (2012a). Advection transport of river pollutants with bidirectional diffusion in the plane perpendicular to the direction of flow. *Ochrona Środowiska*, *34*(2): 19–24.

Bielski, A. (2012b). Transport of pollutants in a the river with bi-directional diffusion. *Engineering and Protection of Environment*, *15*(3): 307–332.

Ceka, A. (2011). *Water framework directive and mixing zone guidelines*, Swedish University of Agricultural Sciences, Faculty of Natural Resources and Agricultural Sciences, Department of Aquatic Sciences and Assessment, Uppsala.

CORMIX2 (December 1991). *An Expert system for hydrodynamic mixing zone analysis of conventional and toxic multiport diffuser discharges*, EPA/600/3--91/073.

Directive (2008/105/EC) of the European Parliament and of the Council on environmental quality standards in the field of water policy, amending and subsequently repealing Council Directives 82/176/EEC, 83/513/EEC, 84/156/EEC, 84/491/EEC, 86/280/EEC and amending Directive 2000/60/EC of the European Parliament and of the Council.

Directive (2013/39/EU) of the European Parliament and of the Council of 12 August 2013 amending Directives 2000/60/EC and 2008/105/EC as regards priority substances in the field of water policy.

Donnell, B.P., Letter, J.V., McAnally, W.H., et. al. (2011). *Users Guide for RMA2*, Version 4.5. Retrieved from: http://citeseerx.ist.psu.edu/viewdoc/download?doi=10.1.1.369.548&rep=rep1&type=pdf (access: 10.02.2021.

Frick, W.E., Roberts, P.J.W., Davis, L.R., Keyes, J., Baumgartner, D.J., George, K.P. (2003). *Dilution models for effluent discharges (Forth Edition)*, EPA/600/R-03/025, Surface Water Models. Retrieved from: https://www.epa.gov/exposure-assessment-models/surface-water-models (access: 10.02.2021).

HEC – RAS (2016). *River analysis system.* Version 5.0, US Army Corps, Hydrologic Engineering Center.

Holtschlag, D.J., Koschik, J.A. (2002). *A two-dimensional hydrodynamic model of the St. Clair and Detroit Rivers within the Great Lakes Basin*, U.S. Geological Survey Water Resources Investigations Report 01-4236. Retrieved from: http://mi.water.usgs.gov/pubs/WRIR/WRIR01-4236/ (access: 10.02.2021).

Jirka, G.H., Bleninger, T., Burrows, R., Larsen, T. (2004). *Environmental Quality Standards in the EC-Water Framework Directive: Consequences for Water Pollution Control for Point Sources*, European Water Association.

Kundu, P.K., Cohen I.M. (2002). *Fluid mechanics*, Academic Press.

Martin, J.L., McCutcheon S.C. (1999). *Hydrodynamics and transport for water quality Modeling*, CRC Press, Inc.

Myung Eun Lee, Il Won Seo (2010). 2D Finite element pollutant transport model for accidental mass release in rivers. *KSCE Journal of Civil Engineering*, *14*(1): 77–86.

Pinho, J., Rui Ferreira R., Vieira, L., Schwanenberg, D. (2015). Comparison Between Two Hydrodynamic Models for Flooding Simulations at River Lima Basin. *Water Resource Management*, 29: 431–444.

Ramaswami ,A., Milford, J.B., Small, M.J. (2005). *Integrated environmental modeling*, John Wiley & Sons.

Rutherford, J.C. (1994). *River mixing*, John Wiley & Sons.

Surface-water Modeling System. Retrieved from: https://www.aquaveo.com/software/sms-riverine-flood-modeling (access: 10.02.2021).

Technical Background Document on Identification of Mixing Zones, Brussels, December 2010.

Technical guidelines for the identification of mixing zones, Brussels, 22 December 2010.
Vedat Batu (2006). *Applied flow and solute transport modelling in aquifers – Fundamental principles and analytical and numerical methods*, Taylor & Francis Group.
Wesseling, P. (2000). *Principles of computational fluid dynamics*, Springer-Verlag, Berlin, Heidelberg, New York.

https://doi.org/10.37705/TechTrans/e2021004